A Study on Distance Measurement System Based on Low -Coherence Interferometry

Ruiping Wang, Xiaomei He, Jiajia Dong, Xiangyu Cai, Xueyi Zhang
Changcheng Institute of Metrology and Measurement(CIMM), Beijing, China

Abstract: A fiber-optic low-coherence interferometry system capable of absolute distance measurement is proposed. Light emitted from a broadband light source is split by a fiber-optic Michelson interferometer. When the optical path difference between the measurement arm and the reference arm falls within the coherence length of the light source, interference occurs. By demodulating the interference signal, the zero optical path difference (ZOPD) position can be obtained. The reference mirror is mounted on a reference arm translation stage to scan and locate the ZOPD positions of different measurement surfaces. By extracting the ZOPD position of each measurement surface, the absolute distance value can be obtained. The designed system features a simple structure, fast measurement speed, and high measurement accuracy. The measurement repeatability is better than 1 μm, and the measurement range exceeds 6 mm.

Keywords: Low-coherence Interferometry, Michelson Interferometer, Distance Measurement, Signal Demodulation

1. Introduction

Laser interferometry distance measurement technology leverages the high directionality, high monochromaticity, and high brightness of lasers to enable non-contact, long-range measurements. It can be used for online measurement of parameters such as length, angle, and rotational speed. Fiber-optic Low-coherence Interferometry Distance Measurement systems possess the advantages of high precision and non-contact measurement, similar to laser interferometry distance measurement systems. However, unlike laser interferometry, which requires a high-precision scanning guide rail at least larger than the measured dimension to obtain relative displacement measurements, low-coherence interferometry can directly measure the distance between any two points. It eliminates the need for a measurement guide rail between the two measurement points and does not require the target object (target mirror) to move continuously along the guide rail, enabling absolute measurements. Table 1 presents a comparison between Low-coherence Interferometry Distance Measurement and laser interferometry distance.

Table 1. Comparison of Low-Coherence Interferometry and Laser Interferometry Distance Measurement

	Low Coherence Interference Distance Measurement	Laser Interference Distance Measurement
Light Source	Broad -spectrum light source	Narrow -spectrum laser
COHERENCE LENGTH	μm magnitude	m/km magnitude
Type of Measurement	Absolute Displacement	Relative Displacement
Phase Ambiguity of λ/2	No	Yes
Measurement Dynamic Range	Large	Small
Anti-interference Ability	Strong, measurement results are not affected by the stability of the light source wavelength and power	Weak, measurement results are affected by the stability of the light source wavelength

Furthermore, Low-coherence Interferometry Distance Measurement systems overcome the limitation of laser interferometry systems, where the measurement dynamic range is restricted to half a wavelength due to the λ/2 phase ambiguity in the interference signal. In contrast, the measurement range of

low-coherence interferometry is not limited by the wavelength of the light wave.

2. Principle of Low Coherence Interferometry

According to the two-beam interference theory [1,2], when two monochromatic light beams with specific wavelengths undergo strong coherent interference, the intensity of the interference light produced by a Michelson interferometer can be expressed as [3].

$$I = A_0 + A_1 cos\delta = A_0 + A_1 \cos\left(\frac{2\pi\Delta}{\lambda}\right) \quad (1)$$

Where $\Delta = nl$ represents the optical path difference between the two beams, A_0 is the DC component of the interference, A_1 is the visibility of the interference signal, δ is the phase difference between the two beams, and λ is the wavelength of the light source. According to Equation (1), the relationship between the intensity of the strongly coherent interference and the optical path difference is shown in Figure 1(a). It can be seen that when a narrowband light source is selected, the resulting interference intensity exhibits a sinusoidal distribution. The amplitude of the intensity does not change with the variation of the optical path difference and remains constant, making it impossible to obtain the change in optical path difference through demodulation. Therefore, it does not have any localization detection function.

For low-coherence interferometry, due to the finite bandwidth of the broadband light source, the interference intensity can be considered as the superposition of the interference of monochromatic light of all wavelengths. In this case, in Equation (1), λ represents all the wavelengths of the broadband light source, and the expression for the interference intensity becomes an integral with the variation range of λ as the upper and lower limits of integration, as shown in the following equation:

$$I = A_0 + A_1 \int_{\lambda_0-\lambda_n}^{\lambda_0+\lambda_n} \Phi(\lambda) \cos\left(\frac{2\pi\Delta}{\lambda}\right) d\lambda \quad (2)$$

Where λ_0 is the center wavelength of the broadband light source, λ_n is the spectral width of the light source, and $\Phi(\lambda)$ is the energy distribution of the interference signal with respect to λ. According to Equation (2), the relationship between the intensity of the low-coherence interferometry and the optical path difference is shown in Figure 1(b). When a broadband light source is selected, the resulting interference intensity exhibits a Gaussian-modulated sinusoidal signal. The interference intensity reaches a maximum at the ZOPD position, i.e., the equal path point, and decreases rapidly with increasing optical path difference. Within the coherence range, the contrast of the interference fringes changes significantly, so the low-coherence interferometry system can accurately read the ZOPD position and achieve very high precision localization and measurement.

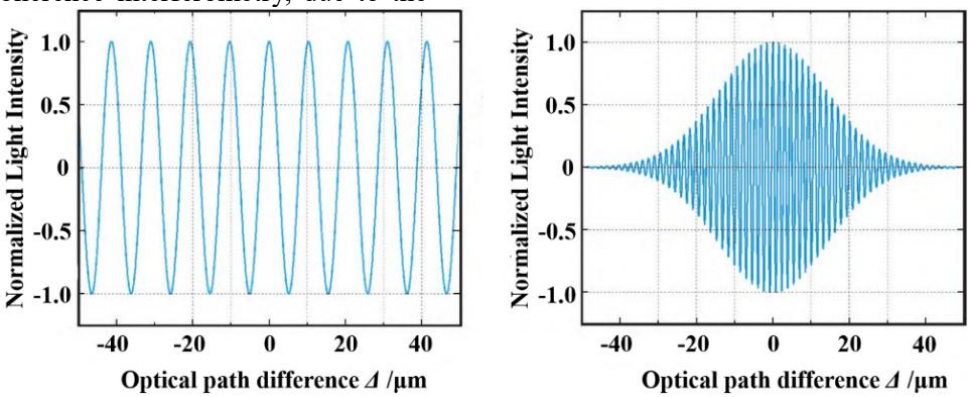

(a) high coherent interference light **(b) low coherent interference light**

Figure 1. The Relationship Between Light Intensity and Optical Path Difference of Different Light Sources

3. System Structure of Low -Coherence Interferometry Distance Measurement

As shown in Figure 2, the Low-coherence Interferometry Distance Measurement system designed and constructed in this paper is based on the principle of the fiber-optic Michelson interferometer. It mainly includes a broadband light source SLD, a 3dB coupler, a reference arm, a measurement arm, a photo detector, a data acquisition card, and an indicator light source. The broadband light

source is a super luminescent diode (SLD) with a center wavelength of 1310 nm and a spectral width of 85 nm. Its coherence length A can be calculated by the following formula:

$$l_c = \frac{2ln2}{\pi}\frac{\lambda_0^2}{\Delta\lambda} \quad (3)$$

Where λ_0 is the center wavelength of the light source and $\Delta\lambda$ is the spectral width, Therefore, the coherence length of this system is 8.9 μm. The photo detector is an InGaAs photo detector with a detection wavelength range of 800 nm to 1700 nm, used to collect low-coherence interferometry signals and convert the interference optical signal into an electrical signal. The data acquisition card is a multi-channel high-speed data acquisition device used to simultaneously acquire signals from the displacement stage and the photo detector. The indicator light source is a laser diode (LD) with a wavelength of 660 nm.

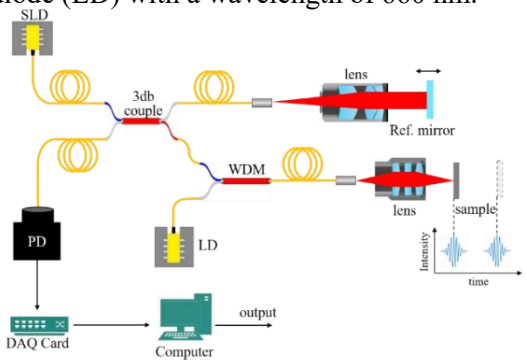

Figure 2. Schematic Diagram of Low-coherence Interferometry Distance Measurement System

The light emitted from the SLD is split into two beams by a 2×2 fiber coupler. One beam is combined with the indicator light in a wavelength division multiplexer (WDM), and then focused onto the sample surface by a fiber measurement mirror. After being reflected by the measured sample, the light returns to the coupler for interference. The LD is used to indicate the measurement position. The other beam is collimated by a fiber collimator and then vertically incident on the reference mirror, then reflected back to the coupler for interference. A high-precision displacement stage drives the reference mirror to locate the ZOPD position of the measured sample surface at different positions. When the optical path difference between the two beams is less than the coherence length of the broadband light source (8.9 μm), low coherence interference occurs. By extracting the ZOPD position of the interference signal, the absolute measurement of the measured distance is realized.

4. Extraction of Interference Signal

The ZOPD in a fiber-optic Low-coherence Interferometry Distance Measurement system corresponds to the position of the maximum envelope peak and contrast in the interference pattern. This is because at this position, all wavelength components of the broadband light source add up in phase. Based on this characteristic of low coherence interference, the ZOPD is typically used to determine the absolute origin in absolute distance measurements.

The low-coherence interferometry signal of a broadband light source is symmetric about the ZOPD position. However, due to the interference of shot noise, relative intensity noise, thermal noise, and other factors [4], the signal-to-noise ratio of the actually measured interference signal is low, which is not conducive to locating and extracting the ZOPD position, thereby affecting the measurement accuracy of absolute distance. In order to better filter out the noise generated during the acquisition process and enhance the signal-to-noise ratio, facilitating signal analysis, this paper first filters the signal broadening caused by the Doppler shift. The relationship between the Doppler frequency of light perpendicularly incident on a moving object and the wavelength and velocity is:

$$f_0 = \frac{2v}{\lambda_0} \quad (4)$$

Where f_0 represents the signal frequency; λ_0 represents the center wavelength of the broadband light source; v represents the running speed of the displacement stage; in the design of this paper, $v = 4mm/s$, $\lambda_0 = 1310nm$, from which it is estimated that f_0 =6.11×10^{3}Hz, and considering that the wavelength range of the broadband light source is 1267.5nm~1352.5nm, the frequency range of the low coherent interference signal is 5.91×10^{3}Hz~6.31×10^{3}Hz. When used in practice, the frequency band can be slightly wider, in this paper, the frequency of the bandpass filter is selected as 5.11kHz~7.11kHz, and the center frequency is 6.11kHz.

Filtering can effectively improve the signal-to-noise ratio of the original signal. The next step is to accurately extract the ZOPD

position. Wavelet transform, with its high precision and noise immunity, is widely used in the analysis and processing of interference signals [5-7].

A wavelet is a family of functions obtained by scaling and translation of a mother wavelet. Let ψ(t) be the mother wavelet, then the wavelet family is [8,9].

$$\psi_{a,\tau}(t) = \frac{1}{\sqrt{a}}\psi\left(\frac{t-\tau}{a}\right) \quad (5)$$

where a is the scaling factor, which changes the center frequency and bandwidth of the sub-wavelet by changing the value of a; τ is the translation factor, which changes the position of the sub-wavelet by changing the value of τ, thereby analyzing the region of interest of the target function.

For any square integrable function *f(t)*, the wavelet transform is defined as

$$WT(a,\tau) = \frac{1}{\sqrt{a}}\int_{-\infty}^{+\infty} f(t)\psi^*\left(\frac{t-\tau}{a}\right)d\tau \quad (6)$$

where $\psi^*(t)$ is the conjugate function of $\psi(t)$.

Since the complex Morlet wavelet is a complex modulated signal with a Gaussian envelope [10], and its expression is very similar to that of a low-coherence interferometry signal, in this paper, the complex Morlet wavelet is used as the mother wavelet to analyze the interference signal. By performing wavelet transform on the interference signal, we obtain

$$WT_f(a,\tau) = WT_{fr}(a,\tau) + jWT_{fi}(a,\tau) \quad (7)$$

Therefore, the envelope of the interference signal obtained using the complex Morlet wavelet is

$$\left|WT_f(a,\tau)\right| = \sqrt{WT_{fr}^2(a,\tau) + WT_{fi}^2(a,\tau)} \quad (8)$$

where $\left|WT_f(a,\tau)\right|$ is the wavelet coefficients, and $WT_{fi}(a,\tau)$ and $WT_{fr}(a,\tau)$ are the imaginary and real parts of the interference signal after the complex Morlet wavelet transform, respectively. By changing the size of τ, the sub-wavelet continuously slides on the target function. When the overlap between the wavelet function and the analyzed interference signal is the highest, the wavelet coefficient reaches the maximum value. By determining the maximum peak position of the wavelet envelope, the ZOPD position of the interference signal can be located, and the distance can be calculated by finding the difference between the two maximum peak positions of the low coherent interference signal.

Based on the aforementioned theory and analysis, the interference signal of each individual measurement point was demodulated, and the results are shown in Figure 3.

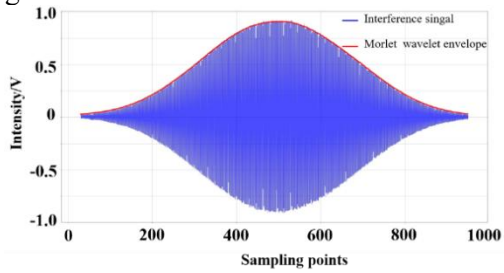

Figure 3. Interference Signal and Morlet Wavelet Envelope of Single Measured Point

5. Experiment and Analysis

5.1 Measurement Repeatability Experiment

To ensure the reliability of measurement results, a step gauge with a calibrated height of 1.0099 mm was used as the test sample to evaluate the system's measurement repeatability. Ten repeated measurements were conducted at fixed points on both the lower and upper surfaces of the step gauge. The interference signals obtained from the two surfaces were processed using the complex Morlet wavelet transform to obtain the distance values (x_i) of the lower and upper surfaces of the step gauge. The measurement repeatability of this system is characterized by the standard deviation (σ) of the ten measurements. Figure 4 shows the interference signal and its envelope from a typical measurement.

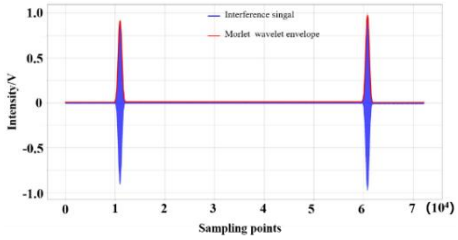

Figure 4. Distance Measurement Interference Signal and Morlet Wavelet Envelope

The standard deviation σ was calculated using Bessel's formula:

$$\sigma = \sqrt{\frac{\sum_{i=1}^{n}(x_i-\bar{x})^2}{n-1}} \quad (9)$$

where x_i is the ith measurement, i=1, 2, 3 ....., 10, $\bar{x}$ is the arithmetic mean of 10 measurements, and n is the number of

measurements.

As shown in Table 2, the average measurement value is 1.0111 mm. The standard deviation of the 10 measurements is 0.9 μm, and the maximum fluctuation is 2.7 μm. These results indicate that the system has high measurement accuracy, stability, and repeatability, meeting the requirements for micrometer-level measurements.

Table 2. System Measurement Repeatability Test Results

Serial No.	Metered Value/mm	Measured Value/mm	Error/μm
1	1.0099	1.0104	0.5
2	1.0099	1.0108	0.9
3	1.0099	1.0113	1.4
4	1.0099	1.0095	-0.4
5	1.0099	1.0104	0.5
6	1.0099	1.0115	1.6
7	1.0099	1.0121	2.2
8	1.0099	1.0112	1.3
9	1.0099	1.0120	2.1
10	1.0099	1.0122	2.3

5.2 Measurement Range Experiment

A reflector mounted on a high-precision displacement platform was used as the test sample. By moving the reflector along the beam direction and performing continuous measurements on the reflector surface, the maximum achievable measurement distance was determined, representing the measurement range of the system. Five measurements were conducted, and the results are shown in Table 3. The maximum measurable distance exceeded 6 mm, indicating that the system has a measurement range of over 6 mm. This demonstrates that the system can be used to measure distances/displacements of up to 6 mm and samples with height/depth variations of up to 6 mm.

Table 3. System Measurement Range Test Results

Serial No.	Displacement/mm
1	6.002
2	6.001
3	6.023
4	6.005
5	6.026

6. Conclusion

In this paper, a fiber-optic low-coherence interferometry system based on a Michelson interferometer is designed and constructed for absolute distance measurement. The complex Morlet wavelet transform is employed to demodulate the low-coherence interferometry signal, and the absolute measurement is achieved by obtaining the difference between the two peak psitions of the interference signal. Experimental results show that the system exhibits high measurement accuracy, with a standard deviation of 0.9 μm for 10 repeated measurements, and a measurement range exceeding 6 mm. The measurement system is simple and has strong anti-interference capability, enabling the measurement of various physical quantities such as displacement, distance, diameter, surface profile, pressure, and vibration. In this paper, a front-view probe is designed for the measurement arm, which limits its application. To expand the application range, the system can be combined with different types of probes, such as side-view probes, rotating probes, and scanning galvanometer probes, depending on the specific application scenario. Moreover, the system can be integrated with rotary tables, displacement stages, and other testing equipment to conduct extensive tests on geometric parameters.

References

[1] Gordon S. Kino, Stanley S. C. Chim. Mirau correlation microscope. Applied optics, 1990, 29(26)：3775-3783.

[2] Lihong V. Wang, Hsin-i Wu. Biomedical Optics: Principles and Imaging[M]. John Wiley & Sons, Inc (2009).

[3] Heming Wei, Kaixing Liao, Xuefeng Zhao, et al. Low-coherent fiber-optic interferometry for in situ monitoring the corrosion-induced expansion of pre-stressed concrete cylinder pipes. Structural Health Monitoring. 2019,18(5-6), 1862-1873.

[4] XU K H, LIANG Y M, WANG J Y, et al. Noise Analysis and Experimental Study of Time Domain Optical Coherence Tomography. Acta Photonica Sinica, 2011, 40(3): 344-349.

[5] R. Recknagel. G. Notni. Analysis of white light interferograms using wavelet methods. Optics Communications. 1998, 148(1-3), 122-128.

[6] P. Sandoz. An algorithm for profilometry

by white light phase shifting interferometry. Journal of Modern Optics, 1996, 43(8), 1545-1554.

[7] R. Dandliker, E. Zimmerrnann, G. Frosio. Electronically scanned white-light interferometry: a novel noise-resistant signal processing. Optics Letters, 1992, 17(9),679. 679-681.

[8] Li Baosheng, Liu Yong, Zhai Yufeng & Wang An, Wavelet method for processing white light interferogram from optical fiber interferometer. Optoelectronics Letters, 2006, 2, 75–77.

[9] Jiwen Cui, Yizhao Niu, Hong Dang, et al. Demodulation Method of F-P Sensor Based on Wavelet Transform and Polarization Low Coherence Interferometry. Sensors. 2020, 20(15), 4249-4266.

[10] Morlet J, Arens G, Fourgeau E, et al. Wave propagation and sampling theory: part I: Complex signal and scattering in multilayered media. Geophysics, 1982, 47(2): 203-221.

